Engineering 17 (2022) 82–92

Contents lists available at ScienceDirect

Engineering

journal homepage: www.elsevier.com/locate/eng

Research
Metamaterials—Article

The Tessellation Rule and Properties Programming of Origami Metasheets Built with a Mixture of Rigid and Non-Rigid Square-Twist Patterns

Jiayao Ma [a,b,#], Shixi Zang [a,b,#], Yan Chen [a,b,*], Zhong You [c,*]

[a] Key Laboratory of Mechanism Theory and Equipment Design of the Ministry of Education, Tianjin University, Tianjin 300350, China
[b] School of Mechanical Engineering, Tianjin University, Tianjin 300350, China
[c] Department of Engineering Science, University of Oxford, Oxford OX1 3PJ, UK

ARTICLE INFO

Article history:
Received 28 September 2021
Revised 28 January 2022
Accepted 17 February 2022
Available online 8 June 2022

Keywords:
Origami metamaterials
Metasheets
Square-twist pattern
Non-periodic tessellation
Programmability

ABSTRACT

Metamaterials constructed from origami units of different types and behaviors could potentially offer a broader scope of mechanical properties than those formed from identical unit types. However, the geometric design rules and property programming methods for such metamaterials have yet to be extensively explored. In this paper, we propose a new kind of origami metasheet by incorporating a family of different square-twist units. The tessellation rule of these metasheets is established to allow compatible mountain–valley crease assignments and geometric parameters among neighboring units. We demonstrate through experiments that the energy, initial peak force, and maximum stiffness of the metasheets can be obtained by a summation of the properties of the constitutional units. Based on this, we are able to program the mechanical properties of the metasheets over a wide range by varying the types and proportions of the units, as well as their geometric and material parameters. Furthermore, for a metasheet with a fixed number of units, all the geometrically compatible tessellations can be folded out of the same pre-creased sheet material by simply changing the mountain–valley assignments, thereby allowing the properties of the metasheet to be re-programmed based on specific requirements. This work could inspire a new class of programmable origami metamaterials for current and future mechanical and other engineering applications.

1. Introduction

Mechanical metamaterials are human-made architected materials with exotic physical properties that are rarely available in natural materials. The behaviors of these metamaterials are dictated by both their microstructures, also known as units, and their material constituents, which can be designed to acquire programmable and tunable properties [1–3]. Initially, rationally designed mechanical metamaterials were developed to generate auxeticity (i.e., a negative Poisson's ratio) [4–7]. With the rapid advances in design methods and additive manufacturing, a variety of counterintuitive mechanical properties have emerged, including bi- and multistability [8–11], tunable thermal expansion coefficient [12,13], pentamode behaviour [14], high specific stiffness [15,16], programmable stiffness [17,18], and *in situ* stiffness manipulation [19].

Origami, the art of folding a two-dimensional (2D) sheet into a three-dimensional (3D) sculpture following a pattern that is a set of mountain and valley creases, offers an elegant and efficient way of constructing metamaterials due to its superior capability for shape transformation, abundance of existing patterns with systematically variable design parameters, and ease of manufacture. Depending on the deformation characteristics, origami can be divided into two categories: rigid origami and non-rigid origami. In the former, the facets surrounded by creases rotate about the creases in the folding process without any deformation within themselves. Consequently, the mechanical response of rigid origami is dictated by the individual creases. The Miura-ori and its derivatives are among the most-adopted rigid origami patterns in the design of metamaterials [20–23]. Despite their simplicity, rigid origami patterns have an inherent limitation: The sole energy

* Corresponding authors.
E-mail addresses: yan_chen@tju.edu.cn (Y. Chen), zhong.you@eng.ox.ac.uk (Z. You).
[#] These authors contributed equally to this work.

https://doi.org/10.1016/j.eng.2022.02.015

input from crease rotations leads to a band of relatively low stiffness. This disadvantage can be somewhat mitigated by means of slight modification to the pattern, such as the introduction of imperfection [17,24] or geometric gradients [23,25]. But a resultant side effect is that the generic folding behavior of the pattern—and the subsequently rigorous theoretical model of the rigid origami and programmability of its properties—is lost. Non-rigid origami involves both facet distortion and crease rotation during folding. Typical examples include origami structures using the Kresling pattern [18,26] and the Resch pattern [27,28]. Facet deformation often substantially contributes to the overall stiffness and enlarges the energy landscape of these metamaterials, resulting in an upper band of mechanical properties, as opposed to those of metamaterials based on rigid origami. Although both rigid and non-rigid origami have been explored in the past, the reported metamaterial designs are usually formed by periodic tessellations of a single type of either rigid or non-rigid origami patterns, and thus are unable to cover the wide range of mechanical properties provided by a possible combination of rigid and non-rigid origami patterns.

To overcome such limitation, we propose a potential design approach that combines rigid and non-rigid origami units within a single metamaterial. By varying the proportion of each type of unit, the mechanical properties can be tuned between an upper limit posed by the non-rigid pattern and a lower limit set by the rigid one. It should be noted that incorporating origami units of different types is generally not trivial, because origami units commonly have different crease numbers and mountain–valley assignments and thus may not be compatible with each other. For this reason, existing origami metamaterials are largely constructed by tiling identical units or units with the same crease patterns but different geometric parameters [23,29]. However, there exists a very rare family of origami patterns known as the square-twist patterns [30–32], which possess an identical crease layout but can have different crease mountain–valley assignments. A change in the crease mountain–valley assignments actually affects how the pattern is folded and, in some cases, the rigidity of folding [33–35]. The identical crease layout makes it possible to tessellate different units together while maintaining geometrical compatibility in the flat and fully folded states. Folding a pattern with such a mixture of units with different rigidities provides ample opportunities to program the mechanical properties.

In this paper, we take advantage of this unique feature of the square-twist patterns and propose a new type of metasheet [30–32]. Previous work [36] has indicated that there are four possible assignments of mountain and valley creases, as shown in Fig. 1, leading to two non-rigid patterns known as types 1 and 2, and two rigid ones referred to as types 3 and 4. Each square-twist pattern has distinct folding behavior and mechanical properties, which have been thoroughly studied at the unit level [37,38]. More recently, metamaterials formed solely by the rigid type-3 pattern have been developed to achieve an adjustable Poisson's ratio [39]. In this paper, we propose the amalgamation of both rigid and non-rigid patterns within a single metasheet, with the aim of programming the metasheet's mechanical properties in terms of energy, load-bearing capability, and stiffness within an elevated landscape by varying the type and proportion of different patterns.

The layout of this paper is as follows. The tessellation rule of the metasheets composed of rigid and non-rigid types of square-twist patterns with different geometric parameters is set up in Section 2. In Section 3, a series of metasheets are designed and fabricated, and quasi-static tension experiments are conducted to obtain the deformation modes and force versus displacement responses. The experimental results are presented and discussed in Section 4. The relationship between the global mechanical properties of the metasheets, the constitutional unit behaviors, and the property programming strategy are also given in this section. Finally, the main findings of the research are summarized in Section 5, which ends the paper.

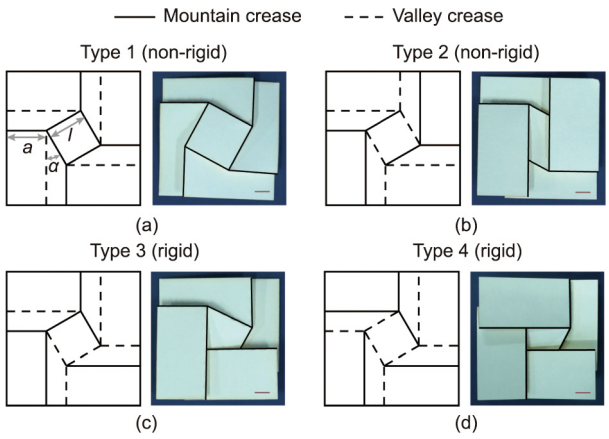

Fig. 1. Crease mountain–valley assignments of four square-twist origami patterns and their folded configurations. (a) Type 1; (b) type 2; (c) type 3; (d) type 4 (scale bar: 5 mm). Mountain and valley creases are described by solid and dashed lines, respectively.

2. Tessellation rule

To obtain the tessellation rule of the metasheets based on the square-twist patterns, we first consider square-twist patterns with an identical layout, defined by side length of square facet l, side length of rectangular facet a, and angle α, as marked in Fig. 1(a). Here, only three types of patterns—the non-rigid types 1 and 2 as well as the rigid type 3 (Figs. 1(a)–(c)) are included in the tessellation. The rigid type-4 pattern is excluded (Fig. 1(d)), since it has a similar mechanical response to type 3. When constructing the tessellation, the three types can be used as units either in the forms shown in Figs. 1(a)–(c) or in their flip-overs—that is, units with reversed mountain–valley crease assignments. It should be noted that the flip-overs of the type-2 and -3 units are equivalent to rotating each unit by 90° and 180°, respectively, whereas the reversed type-1 unit is not. Hence, we treat the reversed type-1 unit, denoted by type 1R, as an independent unit in the tessellation. As a result, we have four units, as shown enclosed in the upper box of Fig. 2(a). Furthermore, since the units have rotational symmetry, if we define those in the upper box of Fig. 2(a) as left-handed units, then their right-handed counterparts, shown enclosed in the lower box, can also be generated. In addition, the left-handed and right-handed versions of the same unit are different, because one cannot be obtained by rotating or flipping the other. Therefore, a total of eight units can be derived from the three types of square-twist patterns: L_i, R_i (i = 1, 2, 3) for the left-handed and right-handed type-1, -2, and -3 units, respectively, plus L'_1, R'_1 for the left-handed and right-handed reversed type-1 units, respectively.

Having obtained the units, we then set up the compatibility condition for those units to be blended together in the flat state. It is apparent from Fig. 2(a) that each edge of the unit has a long and a short crease perpendicular to and intersecting with it. When two units are connected by a common edge side by side, the two short creases intersecting with the common edge must both have the same mountain–valley assignment and be colinear in order to be merged to form a continuous crease, and so should the two long creases. To visualize the connectivity of the units, we introduce a schematic representation that is shown in color in Fig. 2(a). Such a schematic representation was first used in a study of origami patterns formed by degree-4 vertices [29]. Each edge of the unit is represented as a colored serrated line. The arrow-shaped

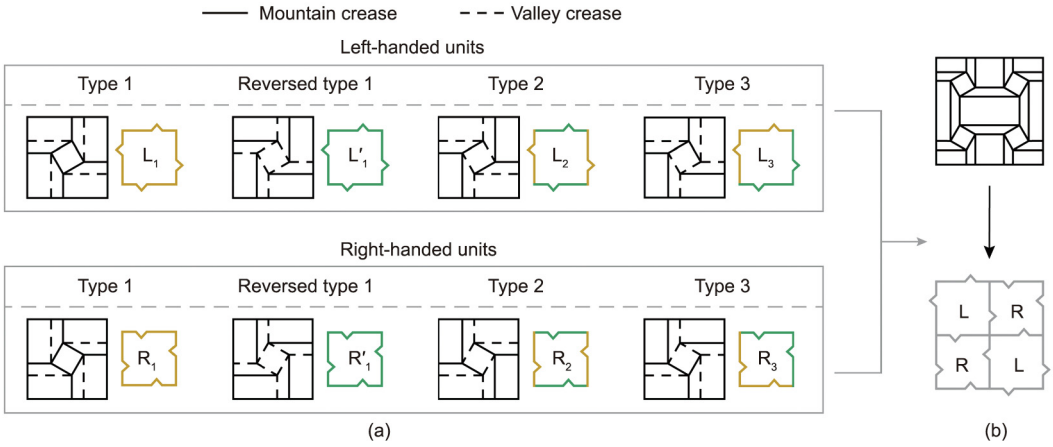

Fig. 2. Tessellation rule of the square-twist units with identical geometric parameters. (a) Mountain–valley assignments and jigsaw puzzle representations of the left-handed and right-handed type-1, reversed type-1, type-2, and type-3 units; (b) a 2 × 2 tessellation defined by left- and right-handed units.

protrusions in the left-handed units and the notches in the right-handed ones indicate the position of the pair of long and short creases. In addition, the yellow color is applied when the short crease is a mountain and the long one is a valley, and the green color when the assignment is opposite. Following this schematic representation, the geometrical compatibility condition dictates that units can be joined only when the connecting edges have an identical color and complementary serrated shapes.

Utilizing the eight units and the tessellation rule, we can design metasheets in a way that is similar to playing a jigsaw puzzle. Starting from square metasheets with 2 × 2 units, it can be seen from Fig. 2(b) that left-handed units must be surrounded by right-handed ones, although the selection of each quarter is not unique. There are four shared edges in the 2 × 2 tessellation, and each one can be either yellow or green, resulting in 16 (2^4) possible combinations. Moreover, in each combination, there are two units to choose from for each piece, resulting in 16 (2^4) possible tessellations. Therefore, the number of all possible 2 × 2 tessellations is 256 ($2^4 \times 2^4$). Excluding those that can be obtained by rotating the others, 136 tessellations are left, which are arranged by the numbers of the type-1-based units (L_1, R_1, L'_1, R'_1) and type-2-based units (L_2, R_2) in Fig. 3. It is notable that the number of type-3-based units (L_3, R_3) can be worked out by subtracting the total of the other two types of units from the number 4. As in the case of creating a single unit, the tessellations fall into two groups that are mirror-symmetric to each other. Another important feature is that all the tessellations share the same crease layout, as shown in Fig. 2(b), and differentiate from each other only by the mountain–valley assignments. This indicates that it is possible to obtain all the designs using the same pre-creased sheet material, and even to transform the metasheet from one design to another by unfolding and refolding. In fact, this feature can be generalized to any $m \times m$ pattern, in which m is a positive integer.

Starting from 2 × 2 tessellations, we can build larger metasheets using either of the following two methods. A straightforward method is to add one unit at a time based on the established tessellation rule. Alternatively, we can use the 136 2 × 2 tessellations as second-order units to create larger tessellations, which is more efficient without missing any design. Theoretically, the number of tessellations increases exponentially with the number of units; thus, $m \times m$ units could produce $2^{m(m+2)}$ square tessellations (see Section S1 in Appendix A for details). While this enables great diversity in the metasheets, it also makes the design process quite complicated. From the viewpoint of mechanical property, nevertheless, it is not necessary to explore all the possibilities. This is because units out of the same type can be treated as identical, since flipping over a unit or changing it from left-handed to right-handed does not affect its folding behavior. Therefore, we can categorize the eight units into three groups—namely, type-1 units including L_1, R_1, L'_1, and R'_1; type-2 units including L_2 and R_2; and type-3 units including L_3 and R_3—and consider only the number of each group in the study of the metasheet's mechanical properties. Consequently, only a small fraction of the vast pool of tessellations with varying unit combinations is required to program the properties of the metasheets. For example, only 15 second-order units are required to design nine 4 × 4 tessellations with varying proportions of type-1 units from 100% to 0 at an interval of 25%, which are shown in Fig. 4. As in the case of 2 × 2 tessellations, all patterns shown in Fig. 4 have the same crease layout, although the mountain–valley assignments differ; that is, a particular crease may be a mountain in one pattern but a valley in another.

In addition to tessellating units with identical geometric parameters, it is possible to introduce geometric gradients in a tessellation. Continue to consider a 2 × 2 tessellation as an example. In the general case, all four units can have different side length l_i and twist angle α_i (i = 1, 2, 3, 4). To satisfy compatibility conditions on the common edges of adjacent units, the geometric parameters of the units shown in Fig. 5 should satisfy the following equations:

$$\begin{aligned} &l_1 \cdot \sin\alpha_1 = l_2 \cdot \sin\alpha_2 = l_3 \cdot \sin\alpha_3 = l_4 \cdot \sin\alpha_4 \\ &a_1^1 = a_3^1,\ a_1^3 + l_1 \cdot \cos\alpha_1 = a_3^3 + l_3 \cdot \cos\alpha_3 \\ &a_1^2 = a_2^2,\ a_1^4 + l_1 \cdot \cos\alpha_1 = a_2^4 + l_2 \cdot \cos\alpha_2 \\ &a_2^3 = a_4^3,\ a_2^1 + l_2 \cdot \cos\alpha_2 = a_4^1 + l_4 \cdot \cos\alpha_4 \\ &a_3^4 = a_4^4,\ a_3^2 + l_3 \cdot \cos\alpha_3 = a_4^2 + l_4 \cdot \cos\alpha_4 \end{aligned} \tag{1}$$

It is important to note that, in the graded tessellation, the four side lengths a_i^1, a_i^2, a_i^3, a_i^4 in a unit are no longer identical, and it is necessary to define them individually. Metasheets with more units can be designed following the same principle.

3. Fabrication and experimentation

To investigate the mechanical properties of the metasheets, physical specimens of the nine 4 × 4 unit tessellations with different unit combinations, as shown in Fig. 4, were fabricated and tested. The unit geometric parameters were set to be $l = a$ = 16.3 mm and α = 30°; thus, the dimensions of the metasheet were 218.8 mm × 218.8 mm in the unfolded state. The specimens were fabricated from 0.4 mm thick polyethylene terephthalate (PET). Along the creases, 0.8 mm × 3.0 mm perforations were made at 1.5 mm intervals using a Trotec Speedy 300 laser-cutting

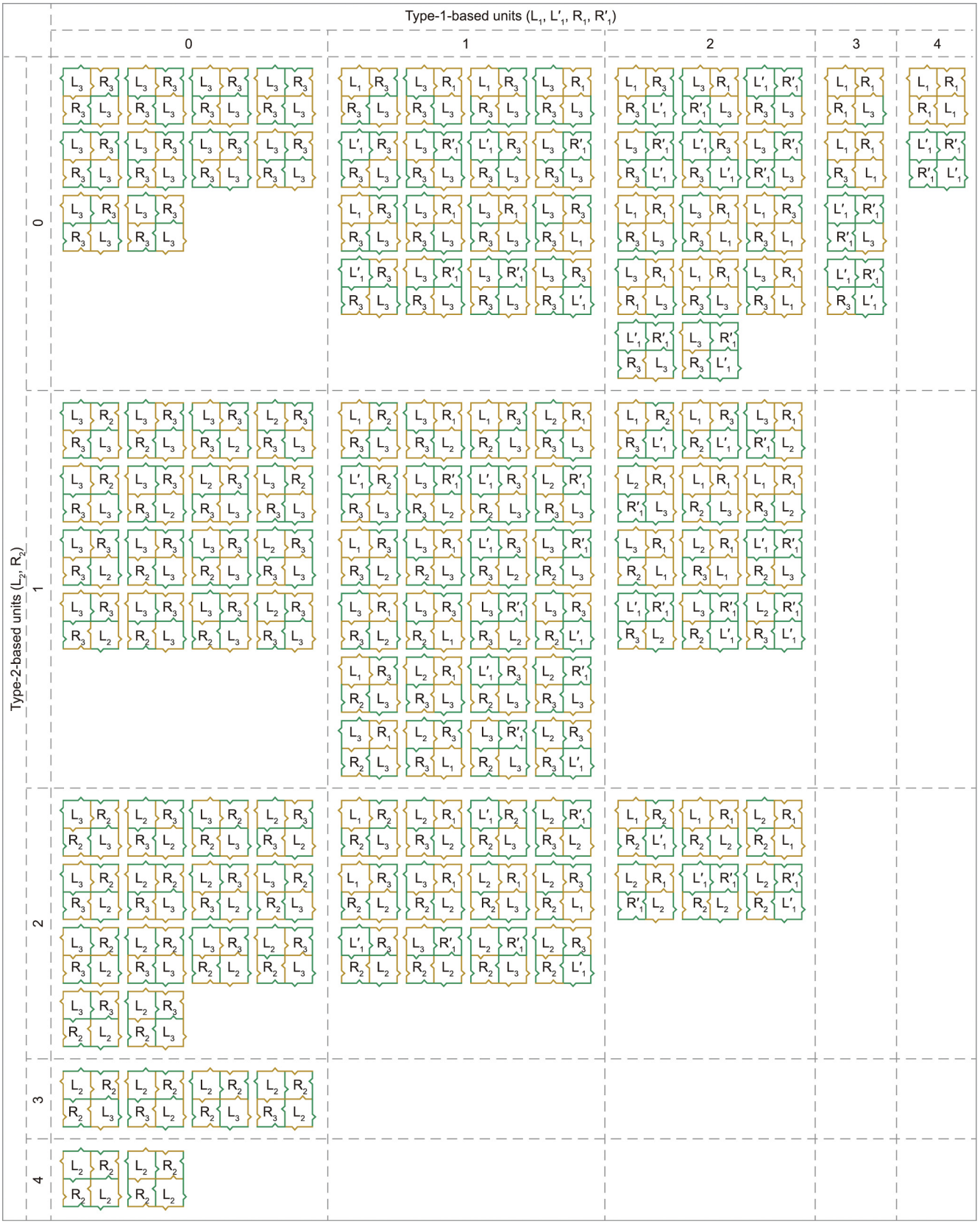

Fig. 3. The 136 2 × 2 tessellations arranged by the numbers of type-1- and type-2-based units.

machine (Speedy 300, Trotec, Austria), as shown in Fig. 6(a). The creases were then produced by manual folding to the fully folded state. Quasi-static tension experiments were conducted on the specimens with a horizontal testing machine developed in-house. The machine had a stroke of 800 mm and a load cell of 300 N. To achieve a uniform deformation, a square loading mechanism

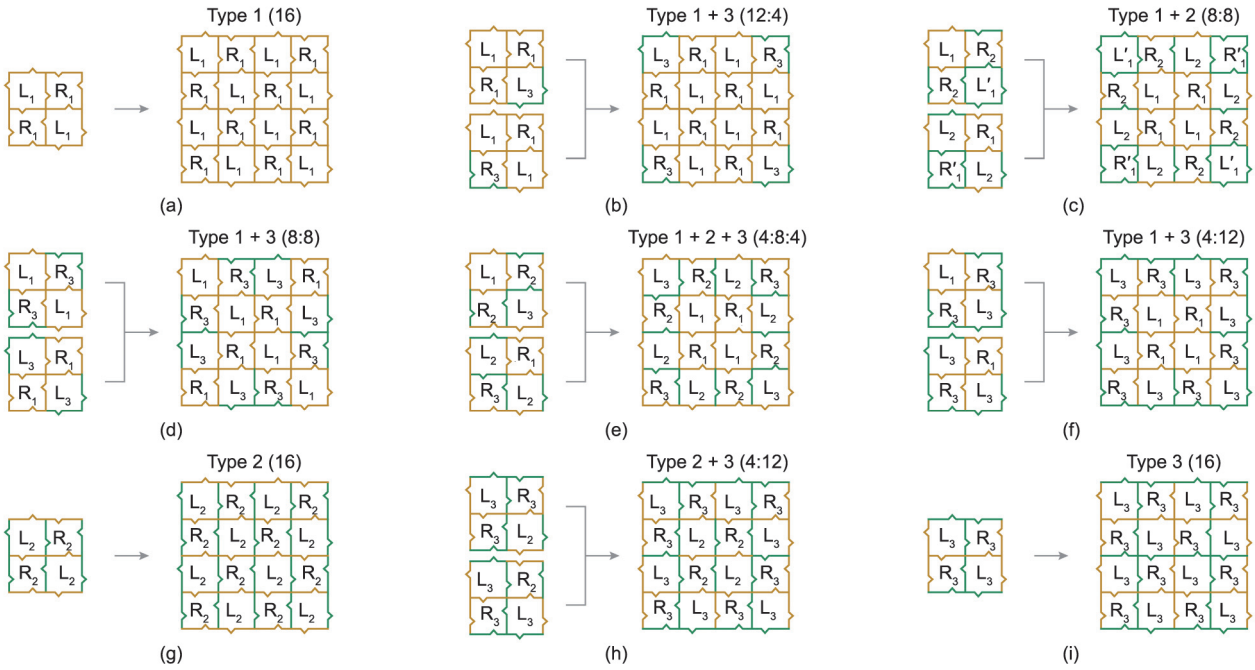

Fig. 4. Nine 4 × 4 tessellations with varying number of type-1 units. (a) 16 type-1 units; (b) 12 type-1 and four type-3 units; (c) eight type-1 and eight type-2 units; (d) eight type-1 and eight type-3 units; (e) four type-1, eight type-2, and four type-3 units; (f) four type-1 and 12 type-3 units; (g) 16 type-2 units; (h) four type-2 and 12 type-3 units; (i) 16 type-3 units.

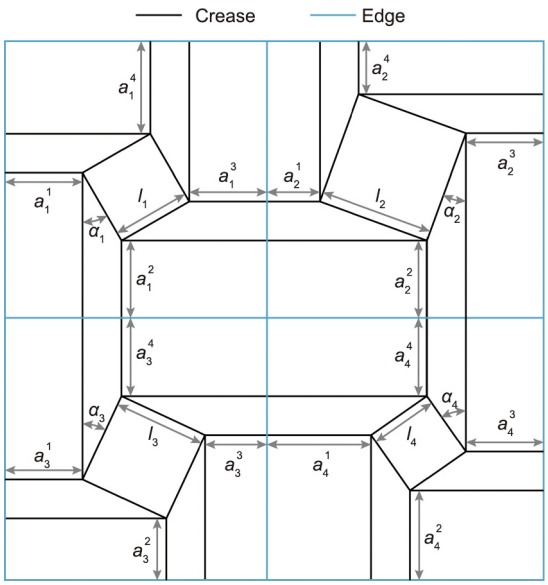

Fig. 5. A 2 × 2 tessellation with geometric gradients.

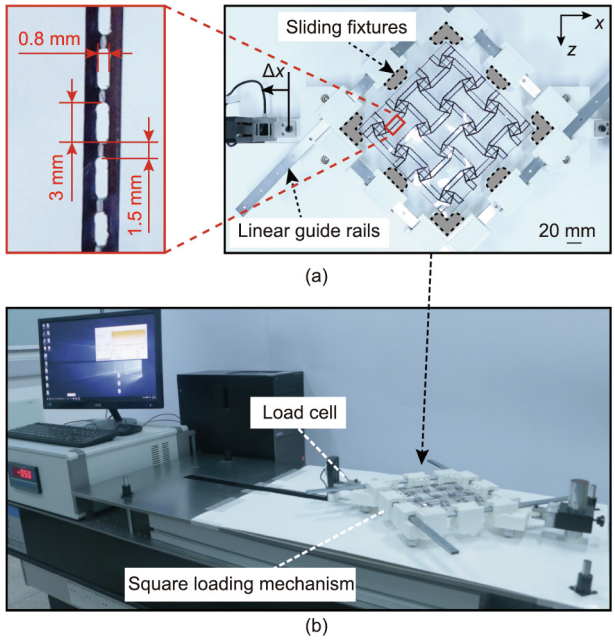

Fig. 6. Tension experiment of the metasheets. (a) Crease design of the specimen and square loading mechanism; (b) experimental setup.

composed of four linear guide rails and eight sliding fixtures was designed to load the specimen at four corners and four middle points of the sides, as shown in Fig. 6(b). Each specimen was stretched at a loading rate of 0.2 mm·s^{-1} until the diagonal length reached 306 mm, at which point the metasheet was nearly completely unfolded and the reaction force rose quickly. The entire deformation process of the specimen was recorded using a digital camera (Canon 70D, Japan) at 25 frames per second, and the force versus displacement curve was extracted from the loading machine. In addition, three key mechanical properties of the unit—the energy U, initial peak force F_{max}, and maximum stiffness K_{max}—were calculated from the curve. The energy was defined as the work done by the force during the loading process, and the maximum stiffness was the largest tangent slope of the force versus displacement curve prior to the initial peak [37]. To obtain reliable results, three specimens were tested for each design.

In addition to the metasheets, individual type-1, -2, and -3 units were also characterized experimentally, following the methods provided in Refs. [37,38]. The unit samples adopted the same geometric parameters and fabrication process as those of the metasheets. The facet bending stiffness and crease rotational stiffness of the units were determined as k_f = 0.70 N·rad^{-1} and k_c = 0.44 N·rad^{-1}, and the yield rotation angle was determined as $\Delta\varphi_y$ = 22.92°. The experimental normalized force (F/k_f) versus the normalized

displacement ($\Delta x/\Delta x_{max}$) curves of the three units are drawn in Fig. 7(a), and the normalized energy $U/(k_f l)$, initial peak force F_{max}/k_f, and maximum stiffness $K_{max}l/k_f$, are presented in Figs. 7(b)–(d). It can be seen that all three properties of the type-1 unit are remarkably greater than those of the type-2 and -3 units. Moreover, the three properties of the type-1 unit are predicted using the empirical formulas in Ref. [37], and those of the type-2 and -3 units using the theoretical formulas in Ref. [38]. As shown in Figs. 7(b)–(d), these predictions match reasonably well with the experimental data, which will later be utilized to program the properties of the metasheets.

4. Results and discussion

4.1. Mechanical properties of uniform metasheets

The deformation processes and normalized force (F/k_f) versus normalized displacement ($\Delta x/\Delta x_{max}$) curves of the three metasheets composed of a single type of unit are presented in Fig. 8. We first investigate the performance of the metasheet formed by the rigid type-3 units. It can be seen from Fig. 8(a) that a simultaneous unfolding of all the units is obtained, leading to a slowly rising force followed by a long plateau. Similarly, the metasheet comprised solely of non-rigid type-2 units shows a synchronized unfolding process among the units, which is shown in Fig. 8(b). As a result, a smooth force curve is generated, as in the case of a single type-2 unit.

Subsequently, we examine the metasheet formed by 16 type-1 units, as shown in Fig. 8(c). In general, the metasheet still exhibits a response similar to that of the individual unit shown in Fig. 7(a), which is characterized by a high initial peak force and a sharp force drop due to the unlocking of the units, followed by a short plateau that is mainly caused by the rotation of the creases. Nevertheless, the units show a noticeable trend of sequential rather than synchronized deformation. To explain this in detail, we classify the units into four groups based on their locations in the tessellation. T_{1-i} units are in the four corners enclosed in the purple boxes; they have two edges joined with surrounding units and two free edges. T_{1-ii} units are on the top and bottom sides of the metasheet enclosed in the yellow boxes; they have three edges joined with those of the neighboring units and are loaded at the long side of the rectangular facets. T_{1-iii} units are on the left and right sides enclosed in the blue boxes; they also have three edges joined with neighboring units but are loaded at the short side of the rectangular facets. Finally, T_{1-iv} units are in the middle enclosed in the red box; they are characterized by four common edges with neighboring units. The deformation of the metasheet can be divided into five stages. At stage 1 from the beginning to configuration I, all the units are stretched simultaneously until the force reaches its initial peak. Subsequently, at stage 2 between configurations I and III, the long rectangular facets formed by the neighboring T_{1-i} and T_{1-iii} units on the left and right sides of the metasheet start to bend inward (configurations II and III), resulting in a slight drop in force. The rectangular facets on the right side bend slightly ahead of those on the left side, probably due to a small geometric imperfection during fabrication. At this stage, all the units are still locked. Upon further loading, the metasheet enters stage 3 bounded by configurations III and IV, where the eight T_{1-ii} and T_{1-iv} units first open up (configuration IV), corresponding to another small peak followed by a sharp drop in force. Afterward, at stage 4 between configurations IV and V, the eight T_{1-i} and T_{1-iii} units (configuration V) pop open, and the force is further reduced. Finally, all the unlocked units are further stretched to flat at stage 5 bounded by configurations V and VI, and the force rises again.

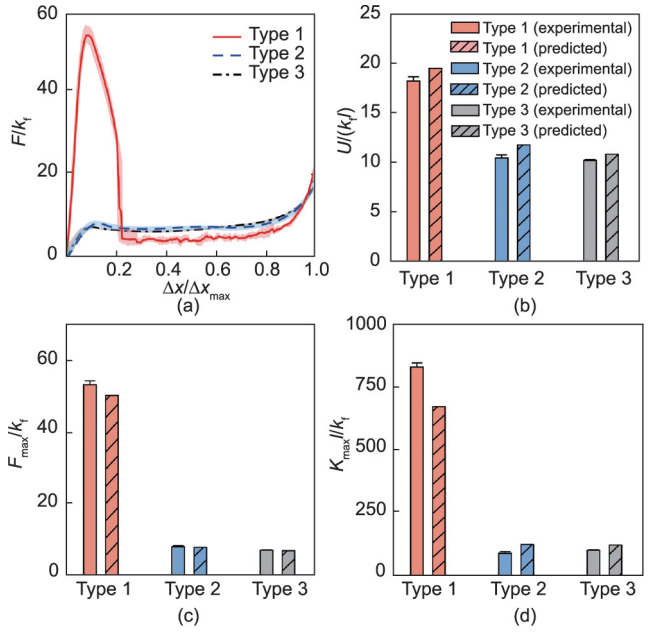

Fig. 7. Mechanical properties of the three types of units. (a) Normalized force (F/k_f) versus displacement ($\Delta x/\Delta x_{max}$) curves. For each curve, the solid line is the averaged result of three tests, and the shaded band is the standard deviation; (b–d) experimental and predicted normalized (b) energy $U/(k_f l)$, (c) initial peak force F_{max}/k_f, and (d) maximum stiffness $K_{max}l/k_f$. The natural dihedral angles formed by the square and trapezoidal facets of the type-1, -2, and -3 units were experimentally determined to be 19.6°, 25.2°, and 28.3°.

To predict the energy, initial peak force, and maximum stiffness of the metasheets, we consider the units as nonlinear springs and the metasheet as an assembly of springs connected in series and parallel. With the predicted unit behaviors in Figs. 7(b)–(d), the predicted energy of the metasheet is the simple summation of unit energies. The predicted initial peak force and maximum stiffness of the metasheet are obtained by adding up those of the units and then dividing them by 4 and 4^2, respectively, since the metasheet has a 4×4 unit arrangement. Fig. 8(g) compares the experimental and predicted results of the three uniform metasheets. In general, there is a reasonably good agreement between the experimental data and predictions. For the metasheet composed of type-1 units, the predictions tend to underestimate the energy. This is mainly caused by the extra bending of the rectangular facets on the left and right sides, which is not observed at the unit level.

4.2. Mechanical properties of mixed metasheets

Having studied the performance of uniform metasheets, in this section we examine the behavior of metasheets formed by a mixture of different units. First, we consider a metasheet based on the design shown in Fig. 4(b) that contains 12 type-1 and four type-3 units in the corners. It can be seen from Fig. 8(d) that a sequential deformation process similar to that of the uniform metasheet with type-1 units is generated. After the initial uniform deformation, the rectangular facets on the left and right sides bend inward; then, the eight T_{1-ii} and T_{1-iv} units open up, followed by the four T_{1-iii} units. In addition, the type-1 units from the same groups as those in the uniform metasheet also tend to deform in the same manner, implying that the behavior of the type-1 unit is mainly determined by its location in the metasheet where the boundary condition is the same. The type-3 units, on the other hand, roughly unfold continuously. Due to the similar deformation process, the force curve is also close in shape to that of the uniform metasheet, but the magnitude is reduced due to the presence of four type-3 units.

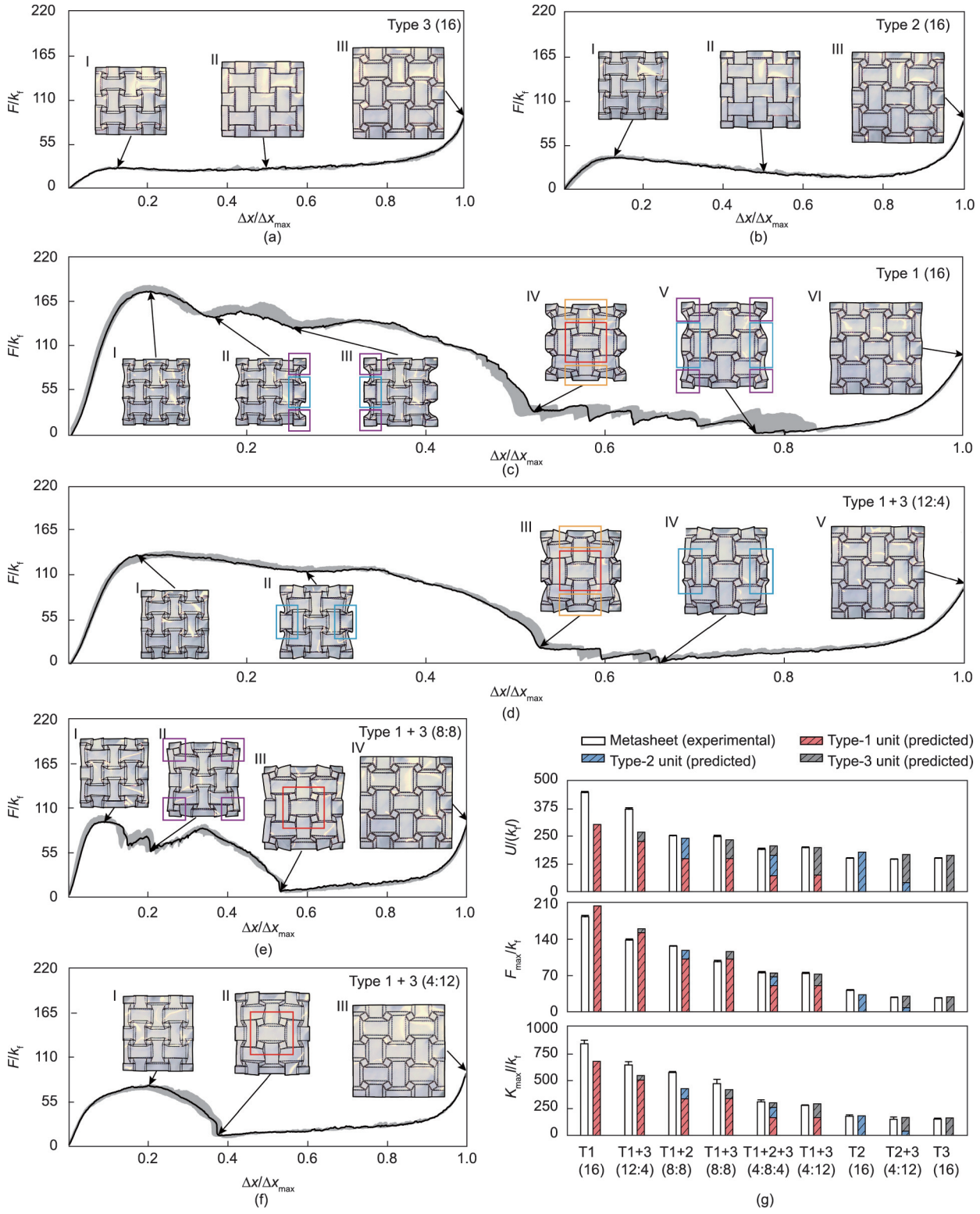

Fig. 8. Deformation processes and mechanical properties of the metasheets. (a–c) Normalized force vs displacement curves and key configurations of the uniform metasheets composed solely of (a) type-3, (b) type-2, and (c) type-1 units, respectively; (d–f) normalized force versus displacement curves and key configurations of the mixed metasheets consisting of (d) 12, (e) eight, and (f) four type-1 units that are supplemented by type-3 units; (g) comparison of normalized energy, initial peak force, and maximum stiffness between the experimental results and predictions. The natural dihedral angles formed by the square and trapezoidal facets of the type-1, -2, and -3 units used in the prediction were experimentally determined to be 19.6°, 20.5°, and 24.3°. T: type.

For a metasheet of the design shown in Fig. 4(d), in which the number of type-1 units is further reduced to eight while the number of type-3 units becomes eight, Fig. 8(e) shows the deformation process. The four T_{1-i} units at the corners, which have fewer constrained edges, pop open in advance of the four T_{1-iv} units in the middle, resulting in two comparable local peaks on the force

curves. A small local peak force occurs between configurations I and II, because the four T_{1-i} units do not open simultaneously. Furthermore, inward bending of the long rectangular facets is no longer evident. For a metasheet consisting of only four type-1 units in the middle surrounded by 12 type-3 units, whose design is given by Fig. 4(f), the type-1 units tend to pop open at the same time, resulting in a force curve similar to that of a single type-1 unit, as shown in Fig. 8(f).

Using the same method, the predicted energy, initial peak force, and maximum stiffness of the six mixed metasheets are calculated. A comparison is made with the experimental data, as shown in Fig. 8(g), from which a good agreement is again observed. Thus, we can safely conclude that the properties of the metasheets can be well predicted by the unit results.

4.3. Properties programmability

Having demonstrated that the energy, initial peak force, and maximum stiffness of the metasheets can be obtained by simply summing up the corresponding unit properties, which are predictable theoretically or empirically, we can now program the material properties of a metasheet through a coarse-stepped tuning by proportioning different units within the metasheet and through a fine continuous tuning by means of geometric and material parameters. To demonstrate this, we consider a series of 4×4 metasheets composed of type-1 and type-3 units, which have identical geometric and material parameters as those in Sections 4.1 and 4.2. The number of type-1 units that play a major role in determining the properties changes from 0 to 16 (see Section S2 in Appendix A for details). Figs. 9(a)–(c) shows the variation of normalized energy, initial peak force, and maximum stiffness of the metasheets. As expected, all three properties increase linearly with the number of type-1 units in a stepped manner. In addition, since all these 4×4 metasheets can be fabricated out of the same crease layout, as demonstrated in Section 2, we can even reprogram a single metasheet in response to specific needs by folding it differently. For example, we can first fold it to the design with only type-3 units to achieve a low force, and then unfold and refold it to the design with only type-1 units to obtain a higher initial force peak. A similar reprogramming/reconfiguring strategy was used at the unit level to design frequency-reconfigurable antennas [32]. With our proposed tessellation designs, the variety and tunable range can be greatly expanded.

By further incorporating the unit geometric and material properties, continuous fine-tuning over a wide bandwidth can be achieved. The effect of varying the side lengths ratio, a/l, in conjunction with the number of type-1 units in the 4×4 metasheets is presented in Figs. 9(d)–(f). It can be seen that increasing a/l within the range of 0.5–4.0 tends to increase all three mechanical properties, regardless of the number of type-1 units. Moreover, any value in between the two adjacent steps in Figs. 9(a)–(c) can be obtained by selecting a/l appropriately. As shown in Fig. 9(a), the normalized energy $U/(k_f l)$ is 223.6 when there are eight type-1 units in the metasheet and becomes 234.4 when there are nine. In order to obtain a $U/(k_f l) = 229.0$, which is the average of the previous two, we can keep eight type-1 units and increase a/l from 1.00 to 1.06, or preserve the number of type-1 units as nine and reduce a/l from 1.00 to 0.94.

The effect of the other geometrical parameter α, is presented in Figs. 9(g)–(i), where α changes from 20° to 45°. Similar to a/l, an increase in α leads to improvements of all three properties. However, the effect of increasing type-1 units on the initial peak force and maximum stiffness is prominent only when α is relatively large and beyond about 30°. This is because, when α is small, the unit is less twisted when folded, resulting in sharp reductions in both initial peak force and maximum stiffness for the type-1 unit.

Finally, the effect of varying k_c/k_f, the ratio of crease rotation stiffness to facet bending stiffness, between 0.25 and 0.75 is presented in Figs. 9(j)–(l). Changing k_c/k_f primarily alters the total energy of the metamaterial and is less effective on tuning either the initial peak force or maximum stiffness. Again, this parameter can be used to obtain any value between the two neighboring steps in Figs. 9(a)–(c), as in the case of a/l and α. It should be noted that, in this discussion, all the units in a metasheet are assumed to have identical geometry and stiffness. Using unit types, design parameters, or a combination of both, it is possible to tailor the properties of the metasheet to meet specific requirements. For example, in order to design an impact energy absorption device, which requires a low initial peak force but high energy absorption, the number of type-1 units should be lowered because doing so results in a high peak, while large values of a/l, α, and k_c/k_f should be selected to maximize the energy absorption.

Unit grading can also be introduced to further enhance the performance of a metasheet. In certain engineering applications, such as non-lethal projectiles for peace-keeping operations, a graded stiffness could enhance the functionality of structures or materials [40]. By purposely introducing a geometric gradient into a metasheet, a sequential deformation mode and a graded response can be engineered. To demonstrate this, a graded 4×4 metasheet consisting of only type-1 units with the dimensions shown in Fig. 10(a) was designed, fabricated, and tested following the procedure outlined in Section 3. Fig. 10(b) shows that the eight units along the left and right sides—which have a small α and thus a lower initial peak force—first open up, followed by the eight middle ones with a larger α. As a result, a graded force response with two consecutive local peaks is obtained. More local peaks can be triggered by increasing the number of units; the position and magnitude of each peak can be programmed as well, based on the properties of the units.

5. Conclusion

We have designed a new group of origami metasheets by amalgamating rigid and non-rigid square-twist origami units into single metasheets and analyzing their energy, load-bearing capability, and stiffness. The tessellation rule for creating such a metasheet has been established in order to satisfy the geometric compatibility conditions among neighboring units of different types and geometric parameters. A series of metasheets with varying unit combinations have been designed, fabricated, and tested. The experimental results indicate that the three types of units can generally maintain their specific deformation modes and corresponding mechanical properties. We have demonstrated that a metasheet can be treated as an assembly of nonlinear springs connected in series and in parallel for the purpose of predicting its energy, initial peak force, and maximum stiffness. The mechanical properties of the metasheet can be obtained simply by summing up the properties of its constitutive units. A good agreement between experimental data and predictions was obtained. Based on this, the mechanical properties of the metasheets can be continuously programmed over a wide range by tuning the proportions of different units within a sheet and the geometric and material parameters of the units. Moreover, all the metasheets with the same layout can be folded out from the same pre-creased sheet, which enables re-programmability by simply folding the sheet following different crease mountain–valley assignments. Our work expands the design scope of origami-inspired metamaterials with a wide range of property programmability and re-programmability to meet practical engineering demands in various fields. Our findings open doors to many interesting future research directions. For example, in order to achieve an automatic and efficient property programming

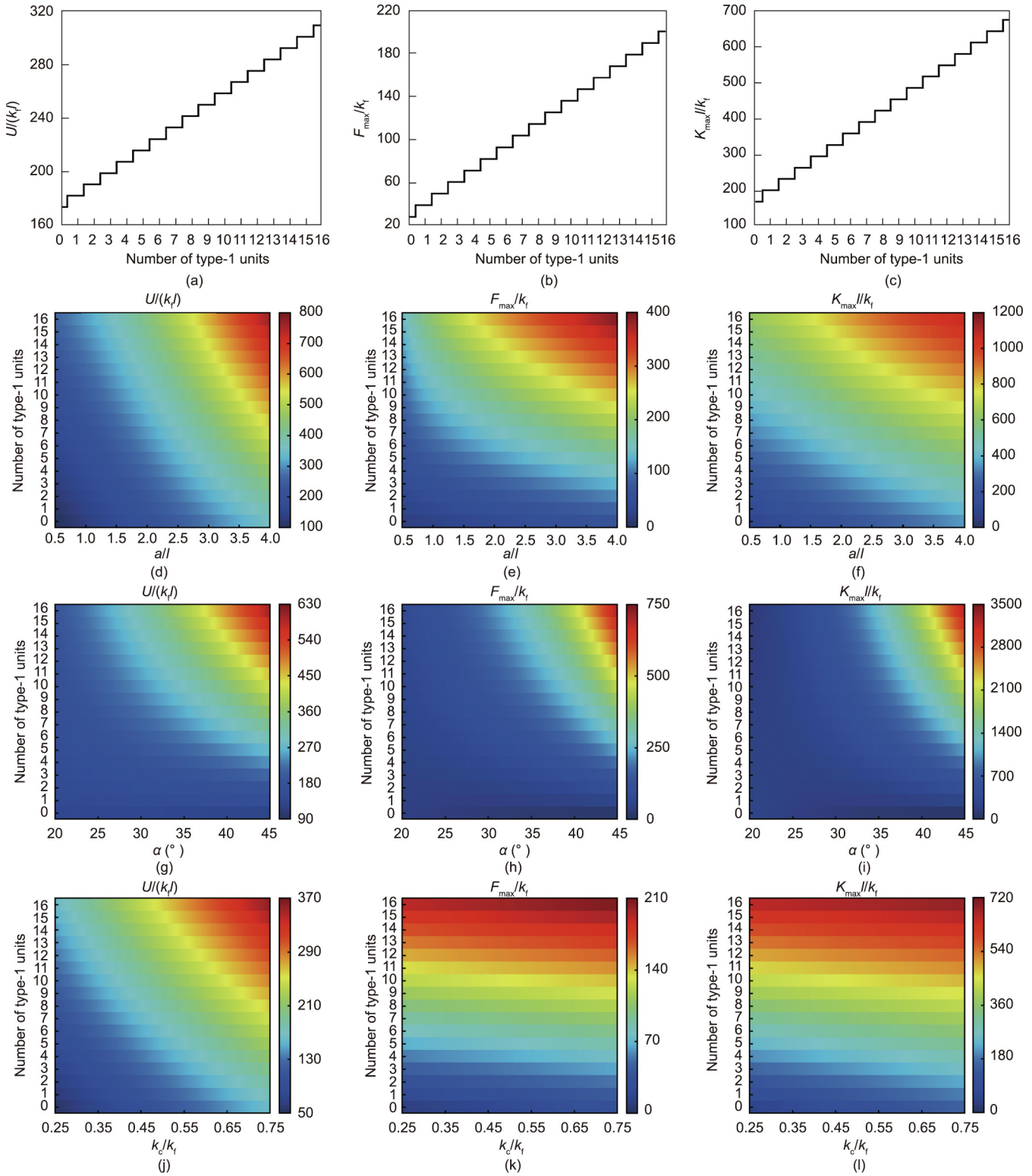

Fig. 9. Programmability of the mechanical properties of 4 × 4 metasheets. (a–c) Normalized (a) energy, (b) initial peak force, and (c) maximum stiffness of the metasheets with varying numbers of type-1 units from 0 to 16; (d–l) normalized energy, initial peak force, and maximum stiffness of the metasheets with varying geometric and material parameters. More specifically, in (d–f), a/l varies from 0.5 to 4.0, while $\alpha = 30°$ and $k_c/k_f = 0.63$; in (g–i), α varies from 20° to 45°, while $a/l = 1$ and $k_c/k_f = 0.63$; and in (j–l), k_c/k_f varies from 0.25 to 0.75, while $a/l = 1$ and $\alpha = 30°$.

process, a machine learning algorithm could be incorporated into what we have discovered in order to more efficiently search for the desired tessellation and design parameters to meet a specific requirement.

Acknowledgments

The work was supported by the National Natural Science Foundation of China (52035008, 51825503, 52192631, and 51721003)

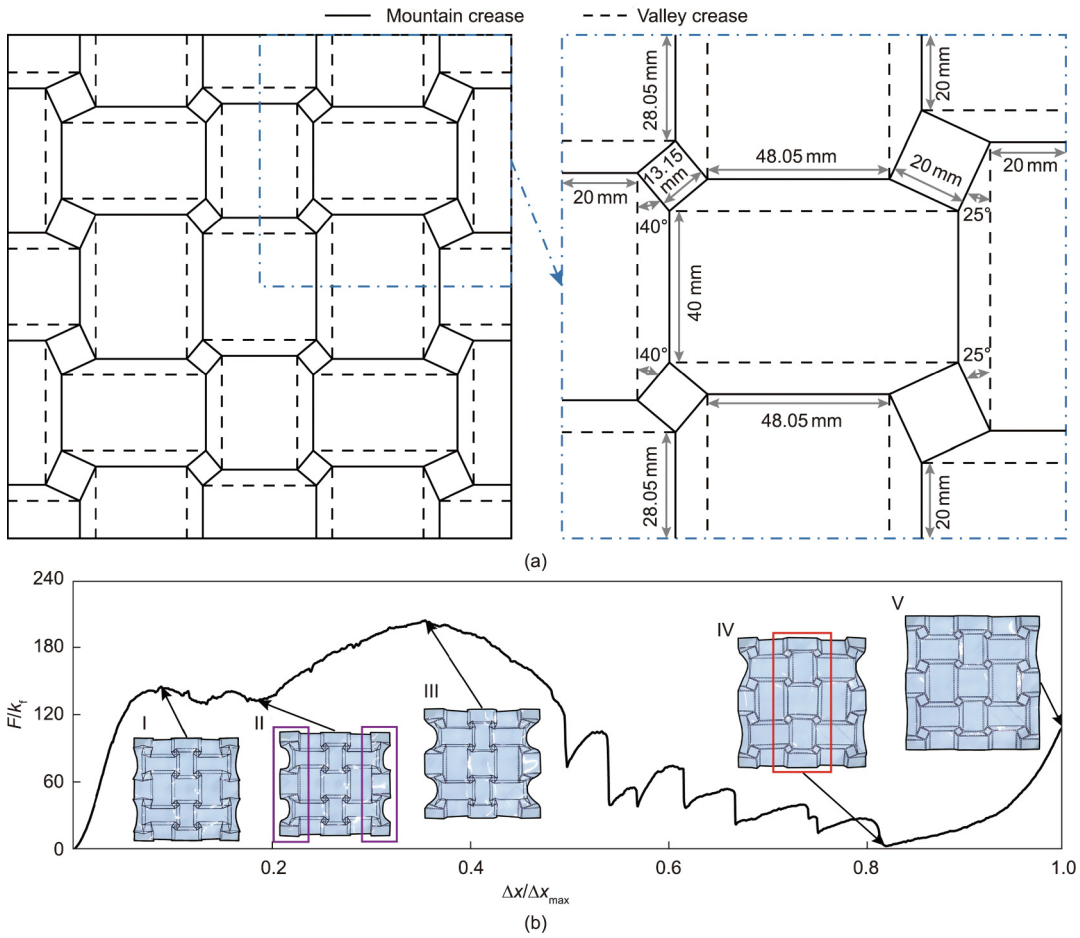

Fig. 10. Graded 4 × 4 metasheet with type-1 units. (a) Pattern and geometric parameters; (b) normalized force versus displacement curve and key configurations.

and the Tencent Foundation (XPLORER-2020-1035). Zhong You's involvement was possible due to the financial support of Department of Engineering Science at Oxford University.

Compliance with ethics guidelines

Jiayao Ma, Shixi Zang, Yan Chen, and Zhong You declare that they have no conflict of interest or financial conflicts to disclose.

Appendix A. Supplementary data

Supplementary data to this article can be found online at https://doi.org/10.1016/j.eng.2022.02.015.

References

[1] Bertoldi K, Vitelli V, Christensen J, van Hecke M. Flexible mechanical metamaterials. Nat Rev Mater 2017;2(11):17066.
[2] Kadic M, Milton GW, van Hecke M, Wegener M. 3D metamaterials. Nat Rev Phys 2019;1(3):198–210.
[3] Liu RP, Ji CL, Zhao ZY, Zhou T. Metamaterials: reshape and rethink. Engineering 2015;1(2):179–84.
[4] Zhang Y, Matsumoto EA, Peter A, Lin PC, Kamien RD, Yang S. One-step nanoscale assembly of complex structures via harnessing of an elastic instability. Nano Lett 2008;8(4):1192–6.
[5] Matsumoto EA, Kamien RD. Elastic-instability triggered pattern formation. Phys Rev E 2009;80(2):021604.
[6] Bertoldi K, Reis PM, Willshaw S, Mullin T. Negative Poisson's ratio behavior induced by an elastic instability. Adv Mater 2010;22(3):361–6.
[7] Matsumoto EA, Kamien RD. Patterns on a roll: a method of continuous feed nanoprinting. Soft Matter 2012;8(43):11038–41.
[8] Brunck V, Lechenault F, Reid A, Adda-Bedia M. Elastic theory of origami-based metamaterials. Phys Rev E 2016;93(3):033005.
[9] Kamrava S, Mousanezhad D, Ebrahimi H, Ghosh R, Vaziri A. Origami-based cellular metamaterial with auxetic, bistable, and self-locking properties. Sci Rep 2017;7(1):46046.
[10] Sengupta S, Li S. Harnessing the anisotropic multistability of stacked-origami mechanical metamaterials for effective modulus programming. J Intell Mater Syst Struct 2018;29(14):2933–45.
[11] Waitukaitis S, Menaut R, Chen BG, van Hecke M. Origami multistability: from single vertices to metasheets. Phys Rev Lett 2015;114(5):055503.
[12] Boatti E, Vasios N, Bertoldi K. Origami metamaterials for tunable thermal expansion. Adv Mater 2017;29(26):1700360.
[13] Ni X, Guo X, Li J, Huang Y, Zhang Y, Rogers JA. 2D mechanical metamaterials with widely tunable unusual modes of thermal expansion. Adv Mater 2019;31(48):1905405.
[14] Zhang L, Song B, Liu R, Zhao A, Zhang J, Zhuo L, et al. Effects of structural parameters on the Poisson's ratio and compressive modulus of 2D pentamode structures fabricated by selective laser melting. Engineering 2020;6(1):56–67.
[15] Zheng X, Lee H, Weisgraber TH, Shusteff M, DeOtte J, Duoss EB, et al. Ultralight, ultrastiff mechanical metamaterials. Science 2014;344(6190):1373–7.
[16] Berger JB, Wadley HNG, McMeeking RM. Mechanical metamaterials at the theoretical limit of isotropic elastic stiffness. Nature 2017;543(7646):533–7.
[17] Silverberg JL, Evans AA, McLeod L, Hayward RC, Hull T, Santangelo CD, et al. Using origami design principles to fold reprogrammable mechanical metamaterials. Science 2014;345(6197):647–50.
[18] Zhai Z, Wang Y, Jiang H. Origami-inspired, on-demand deployable and collapsible mechanical metamaterials with tunable stiffness. Proc Natl Acad Sci USA 2018;115(9):2032–7.
[19] Zhai Z, Wang Y, Lin K, Wu L, Jiang H. *In situ* stiffness manipulation using elegant curved origami. Sci Adv 2020;6(47):eabe2000.
[20] Schenk M, Guest SD. Geometry of Miura-folded metamaterials. Proc Natl Acad Sci USA 2013;110(9):3276–81.
[21] Zhou X, Zang S, You Z. Origami mechanical metamaterials based on the Miura-derivative fold patterns. Proc Math Phys Eng Sci 2016;472(2191):20160361.

[22] Eidini M, Paulino GH. Unraveling metamaterial properties in zigzag-base folded sheets. Sci Adv 2015;1(8):e1500224.
[23] Ma J, Song J, Chen Y. An origami-inspired structure with graded stiffness. Int J Mech Sci 2018;136:134–42.
[24] Liu K, Novelino LS, Gardoni P, Paulino GH. Big influence of small random imperfections in origami-based metamaterials. Proc Math Phys Eng Sci 2020;476(2241):20200236.
[25] Yuan L, Dai H, Song J, Ma J, Chen Y. The behavior of a functionally graded origami structure subjected to quasi-static compression. Mater Des 2020;189:108494.
[26] Kidambi N, Wang KW. Dynamics of Kresling origami deployment. Phys Rev E 2020;101(6):063003.
[27] Lv C, Krishnaraju D, Konjevod G, Yu H, Jiang H. Origami based mechanical metamaterials. Sci Rep 2014;4(1):5979.
[28] Chen Z, Wu T, Nian G, Shan Y, Liang X, Jiang H, et al. Ron Resch origami pattern inspired energy absorption structures. J Appl Mech 2019;86(1):011005.
[29] Dieleman P, Vasmel N, Waitukaitis S, van Hecke M. Jigsaw puzzle design of pluripotent origami. Nat Phys 2020;16(1):63–8.
[30] Silverberg JL, Na JH, Evans AA, Liu B, Hull TC, Santangelo CD, et al. Origami structures with a critical transition to bistability arising from hidden degrees of freedom. Nat Mater 2015;14(4):389–93. Corrigendum in: Nat Mater 2015;14:540.
[31] Wang LC, Song WL, Fang D. Twistable origami and kirigami: from structure-guided smartness to mechanical energy storage. ACS Appl Mater Interfaces 2019;11(3):3450–8.
[32] Wang LC, Song WL, Zhang YJ, Qu MJ, Zhao Z, Chen M, et al. Active reconfigurable twistable square-twist origami. Adv Funct Mater 2020;30(13):1909087.
[33] Peng R, Ma J, Chen Y. The effect of mountain-valley folds on the rigid foldability of double corrugated pattern. Mechanism Mach Theory 2018;128:461–74.
[34] Chen Y, Fan L, Bai Y, Feng J, Sareh P. Assigning mountain-valley fold lines of flat-foldable origami patterns based on graph theory and mixed-integer linear programming. Comput Strucy 2020;239:106328.
[35] Chen Y, Yan J, Feng J, Sareh P. Particle swarm optimization-based metaheuristic design generation of non-trivial flat-foldable origami tessellations with degree-4 vertices. J Mech Des 2021;143(1):011703.
[36] Feng H, Peng R, Zang S, Ma J, Chen Y. Rigid foldability and mountain-valley crease assignments of square-twist origami pattern. Mechanism Mach Theory 2020;152:103947.
[37] Zang S, Ma J, Chen Y. Deformation characteristics and mechanical properties of a non-rigid square-twist origami structure with rotational symmetry. 2021. arXiv:2109.12488.
[38] Ma J, Zang S, Feng H, Chen Y, You Z. Theoretical characterization of a non-rigid-foldable square-twist origami for property programmability. Int J Mech Sci 2021;189:105981.
[39] Lyu S, Qin B, Deng H, Ding X. Origami-based cellular mechanical metamaterials with tunable Poisson's ratio: construction and analysis. Int J Mech Sci 2021;212:106791.
[40] Jha DK, Kant T, Singh RK. A critical review of recent research on functionally graded plates. Compos Struct 2013;96:833–49.